Chemical Science

EDGE ARTICLE

View Article Online
View Journal | View Issue

Cite this: *Chem. Sci.*, 2017, **8**, 1642

A full set of iridium(IV) pyridine-alkoxide stereoisomers: highly geometry-dependent redox properties†

Dimitar Y. Shopov,[a] Benjamin Rudshteyn,[ab] Jesús Campos,[ac] David J. Vinyard,[ad] Victor S. Batista,[ab] Gary W. Brudvig[ab] and Robert H. Crabtree[ab]

Received 21st August 2016
Accepted 6th November 2016

DOI: 10.1039/c6sc03758e

www.rsc.org/chemicalscience

We introduce and characterize the complete set of possible isomers of $Ir^{IV}(pyalk)_2Cl_2$ (pyalk = 2-(pyridin-2-yl)propan-2-oate), providing valuable insights on the properties of Ir(IV) species. The pyridine alkoxide ligand strongly stabilizes high oxidation states, essential to accessing the catalytically relevant Ir(IV) state, and results in robust complexes that can be handled under ambient conditions, even permitting chromatographic separation. The redox properties are isomer-dependent, spanning a 300 mV range, rationalized with ligand-field theory and DFT calculations. The reported complexes exhibit very high kinetic inertness against isomerization, despite highly disparate predicted thermodynamic stabilities, presenting a unique opportunity to study all five possible isomeric complexes with the same ligand set.

Introduction

Despite the predicted or confirmed involvement of highly oxidized iridium species in a variety of significant catalytic processes,[1–5] few Ir coordination complexes have been isolated in the oxidation state IV or higher. As a result, most of the properties of these high oxidation states are known only through study of a handful of standalone compounds. Investigations on high-valent Ir compounds have generally consisted only of observations made on transient oxidized species.[6] Therefore, there are significant gaps in our understanding of how variation of the ligand environment impacts the properties of high-valent Ir. The primary difficulty in isolating and studying oxidized Ir species originates from the relatively high electronegativity of Ir – even the most common Ir(IV) species, $IrCl_6^{2-}$, is a fairly strong oxidant with an $Ir^{IV/III}$ potential of 0.91 V *vs.* NHE.[7] Forming isolable high-valent complexes requires ligands which are both strongly donating and highly resistant to oxidative degradation.

A specific example of the impact of this scarcity arose during our groups' work with iridium water-oxidation catalysts (WOCs). We discovered that Ir complexes with one pentamethylcyclopentadienyl (Cp*) and one bidentate chelate ligand (C–N, N–N, or N–O type) are precursors to highly efficient and robust WOCs, which form spontaneously on chemical or electrochemical oxidation.[8–13] Computational and spectroscopic studies indicated that the resulting WOC resting states are much altered from the precursor structure, being oxo-bridged dinuclear compounds (Scheme 1) that retain the chelate ligand but lose Cp* to oxidative decomposition.[5,10,14–16] Despite intensive study, the precise structural identity of the catalytic resting state(s) has not yet been confirmed by small molecule

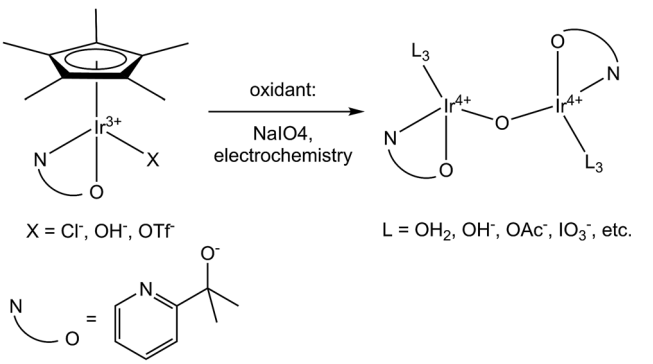

Scheme 1 Transformation of organometallic precursors to highly active water-oxidation catalysts. Proposed catalyst resting state shown on right, accounting for current structural uncertainty.[5]

[a]*Department of Chemistry, Yale University, 225 Prospect St., New Haven, CT 06520, United States*

[b]*Energy Sciences Institute, Yale University, 520 West Campus Dr., West Haven, CT 06516, United States*

[c]*Instituto de Investigaciones Químicas (IIQ), Departamento de Química Inorgánica and Centro de Innovación en Química Avanzada (ORFEO-CINQA), Universidad de Sevilla and Consejo Superior de Investigaciones Científicas (CSIC), Avenida Américo Vespucio 49, 41092 Sevilla, Spain*

[d]*Department of Biological Sciences, Louisiana State University, Baton Rouge, LA 70803, USA*

† Electronic supplementary information (ESI) available: Experimental and theoretical procedures and figures, crystallographic details, and theoretical structures. CCDC 1497501–1497508. For ESI and crystallographic data in CIF or other electronic format see DOI: 10.1039/c6sc03758e

crystallography because suitable crystals cannot be obtained. We suspect that this may be due to the structural variability possible in such dinuclear species; with the combination of variable ligands on the nonchelate sites and diastereomerism means that hundreds of species could form. However, for such variability to persist, the complexes must be substitutionally inert. While the inertness of Ir(III) is well-known,[17,18] there is virtually no published information on the substitution kinetics or other properties of Ir(IV) coordination complexes.

We sought to prepare stable, well-defined Ir(IV) species which would allow us to study this oxidation state. To accomplish this goal, we retained the ligand that gave the most resilient WOC, the pyridine-alkoxide chelate, 2-(pyridine-2-yl)propan-2-oate (pyalk). This ligand was designed to incorporate a number of relevant properties. First, it contains a highly σ and π electron-donating alkoxide arm,[19,20] which not only allows it to stabilize high oxidation states, but also enhances water solubility and permits reversible protonation and hydrogen bonding. Second, this alkoxide is protected from oxidative degradation by the geminal dimethyl substitution, allowing it to survive the harsh reaction conditions required for water oxidation or formation of high-valent metal complexes. Third, alkoxide ligands are normally susceptible to dissociation *via* protonation, especially from reduced metal states, so by pairing the alkoxide with a pyridine we alleviate coordinative instability. The *gem*-dimethyl group (Thorpe-Ingold[21] effect) strongly stabilizes the chelate ring and may help prevent attack from the directions normal to the ligand plane. So long as the pyridyl group remains bound, it seems sterically challenging for the alkoxide arm to be substituted by another ligand even if protonated, as the bulky, cone-shaped $-CMe_2OH$ group blocks the coordination site no matter what rotational conformations are adopted. The alkoxide permits proton-coupling and hydrogen bonding, imparting amphiphilic properties to the ligand and resulting complexes. Finally, the disparity in donor character between the two arms can perturb the overall electronic structure in interesting ways, as we see in the following discussion.

We previously reported[22] on the *mer* and *fac* Ir(pyalk)$_3$ diastereomers, **1** and **2** (Scheme 2), formed together in the same reaction mixtures. Attempted thermal conversion between these isomers revealed that **1** is the thermodynamic product, but that a substantial kinetic barrier hinders isomerization. As we had expected, these complexes readily oxidize to the Ir(IV) state using chemical oxidants like ferrocenium or periodate salts, while solutions of **1** even spontaneously oxidize in air. While both the Ir(III) and Ir(IV) states of these compounds are highly kinetically stable, **1** had a noticeable preference for the oxidized state, while **2** favored the reduced one. Electrochemistry revealed that the two isomers have a striking 340 mV difference in the potential of the $Ir^{IV/III}$ couple. Subsequent work[23] with rhodium echoed these findings – Rh(III) analogues of **1** and **2** shared similar thermodynamic and kinetic properties. The much rarer and elusive Rh(IV) oxidation state was reached by oxidizing the Rh analogue of **1**, resulting in what may be the most stable and best-characterized Rh(IV) complex in the literature. The difference between the two isomers was evident for Rh as well, as the facial complex did not form a stable Rh(IV) species.

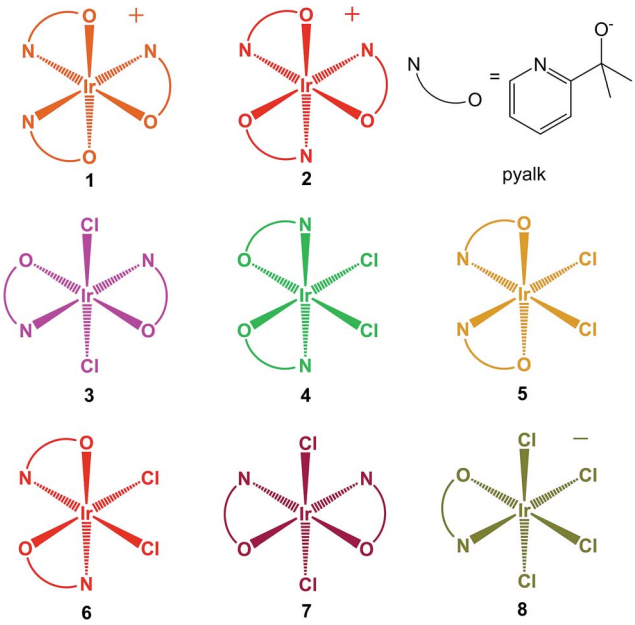

Scheme 2 Structures of the studied Ir-pyalk complexes. Colors approximate the appearance of the compounds' Ir(IV) states.

A redox discrepancy as high as 340 mV is highly unusual for isomers that share the same ligand set, but only differ in their arrangement. Simple treatments, such as Lever parametrization,[19,20,24–26] cannot account for differences due to isomerism. This geometry effect was indeed noted by Lever,[24] but only for strong acceptor ligands (CO, NO^+). More recently, a similar difference has also been observed for Ir compounds with cyclometalated phenylpyridine donor ligands, but the effect was of lower magnitude (≤120 mV).[6] The origin of this anisotropic field oxidation enhancement (AFOE) isomer effect has been discussed briefly by prior authors,[6,24] but has not received significant attention due to the limited number of cases studied and their limited impact. DFT computational work supports our original qualitative explanations and shows that the effect is a result of large donicity disparities in individual ligands around a metal center. The effect is due to ligand-field perturbation of the valence metal d orbitals: since individual d orbitals are anisotropic, they interact most strongly with a subset of the ligands present. If the HOMO of the reduced state is oriented toward one subset of ligands in one isomer and a different subset in another isomer, then unequal interactions with those ligands would result in a different orbital energy for each isomer (see Fig. 1). Since loss of an electron from the HOMO would, therefore, require unequal energy input, each isomer would be expected to undergo oxidation at a different electrochemical potential. This can also be seen as a thermodynamic stabilization of one isomer relative to the other upon oxidation, as one loses a greater sum of antibonding interactions than the other. The greater the discrepancy in donor strength between the different ligands, the greater the difference in these sums can be.

This effect cannot occur in tetrahedral or lower-coordinate ligand geometries, as they lack geometric isomerism, and is

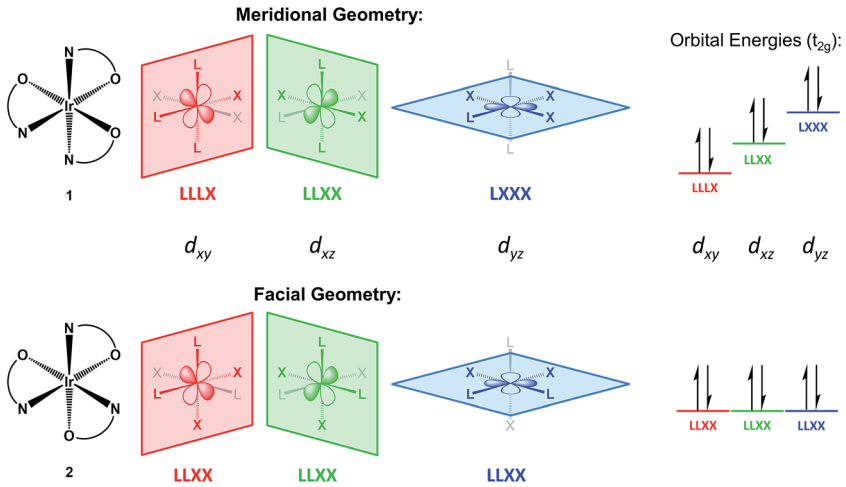

Fig. 1 Effect of ligand arrangement (isomerism) on valence electron energies for the d_π orbitals of a $[ML_3X_3]$-type d^6 low-spin octahedral complex. In this example, ligand X has a higher donor strength than L. The unequal ligand field exerted on the orbitals of the meridional isomer (such as complex **1**) results in a higher HOMO energy than for the facial one (complex **2**), thus lowering the energy needed for one-electron oxidation.

extremely unlikely for square planar geometry, as such isomerism can only perturb the relative energies of the two lowest valence orbitals, d_{yz} and d_{xz}. Therefore, we discuss this effect in terms of octahedral geometry, as it is the most common and also relevant to our examples, although it can also occur in other geometries. In Fig. 1, we illustrate it as it relates to the redox reactions of low-spin d^6 to d^5 complexes, specifically compounds **1** and **2**. In the d^6 Ir(III) state, the three d_π valence orbitals are fully occupied and, thus, inherently degenerate. In the trigonally symmetric facial geometry of **2**, the states remain degenerate. However, in the meridional geometry of **1**, each d orbital is coplanar with a different combination of ligand atoms, thus breaking the degeneracy and elevating one of the orbitals to a higher energy. Since the three d_π orbitals derived from the t_{2g} set collectively interact with all of the ligands, the lowest possible HOMO energy, and thus the least oxidation enhancement, occurs when there is no perturbation at all, as is the case for **2**. On the other hand, the greatest possible enhancement occurs when all of the strong donor ligands are directed towards a single d_π orbital by being coplanar with it, as is the case for **1**. However, fully explaining the magnitude of this difference requires taking account of the donor set, since other *mer*/*fac* isomers with strongly donating LX-type ligands such as phenylpyridine exhibit a much weaker effect.[6] Given the much lower $Ir^{IV/III}$ potentials for the pyalk complexes regardless of isomerism, we conclude that alkoxide is a considerably stronger donor than phenyl, meaning that the pyridine/alkoxide donicity difference is greater than that between phenylene and pyridine in cyclometalated 2-phenylpyridine complexes. Our DFT calculations support this, predicting an approximately 400 mV isomer difference, both *via* the HOMO as well as the thermodynamic differences, a value that is in fact slightly greater than the experimental measurement.[22]

In this report, we expand the family of Ir pyalk complexes by presenting the bis-pyalk species $Ir(pyalk)_2Cl_2$. As a result of introducing a new ligand group, the $N_2O_2Cl_2$ ligand set can give rise to five possible diastereomers, and surprisingly, we have been able to separate and isolate all of them (**3–7**, Scheme 2). Much like **1** and **2**, this rare full set of isomers forms in reactions as mixtures of products that, under proper conditions, contain all five in appreciable yields. These products were readily separated using conventional silica gel chromatography after conversion to the neutral species *via* chemical oxidation to the Ir(IV) state. These oxidized forms of **3–7**, like **1** and **2**, are highly resistant to reduction, decomposition, or isomerization, allowing us a rare opportunity to study a complete set of diastereomers in the uncommon Ir(IV) oxidation state. We characterize and study this set using X-ray crystallography, UV-visible absorption and EPR spectroscopy, electrochemistry, and DFT modeling. One isomer, **3**, is directly analogous to an $Ir(pyalk)_2I_2$ complex from our group isolated by Huang *et al.*[13] which arises from prolonged action of excess free ligand (Hpyalk) on periodate-oxidized Ir WOC.

This series of compounds shows substantially dissimilar $Ir^{IV/III}$ potentials, spanning a total range of over 300 mV; the measured potentials follow the trends expected by our ligand-field model. DFT calculations model the redox trend, correctly ordering the five isomers. In addition, we compute a thermodynamic stability ordering which mirrors the redox order, with the more easily oxidized isomers also being more thermodynamically stable. The difference between the most and least stable isomers is nearly 15 kcal mol^{-1}. Indeed, most energy gaps are predicted to be so large that if product equilibration were fast we would only expect to see one major and one minor isomer. For completeness, we also report on $Ir(pyalk)Cl_4^-$ (**8**), briefly mentioned previously.[27]

Results and discussion

Preparation

Compounds **3–8** were all initially discovered and isolated from reactions between $IrCl_3$ or K_2IrCl_6 and a variable amount (1–2

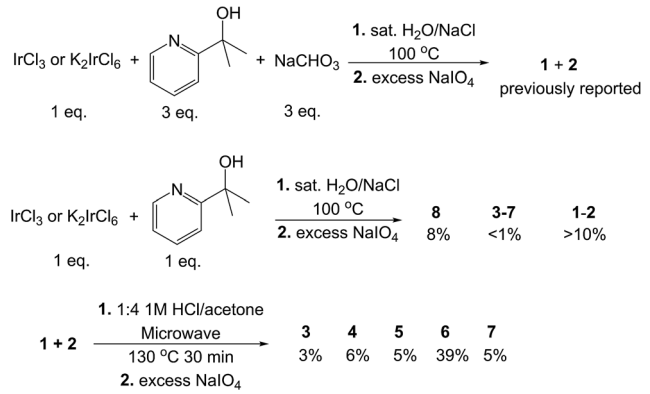

Scheme 3 Reactions used to prepare the studied complexes. Top: route to **1** and **2**.[22] Middle: route to **8**.[27] Bottom: more efficient route to **3–7**.

equiv.) of Hpyalk and (0–2 equiv.) sodium bicarbonate. Subsequent oxidation with sodium periodate to give the less polar Ir(IV) states allowed extraction with dichloromethane, as in the previously reported preparation for compounds **1–2** (Scheme 3). Reducing the amount of ligand and base favored the less ligated species; however, there was a clear bias to forming **1** and **2**, even when just one equivalent of ligand was used with no additional base. In such a 'base-free' reaction, the ligand disproportionates to give, on one hand, the coordinated pyalk Ir species and, on the other, a H_2pyalk^+ counterion paired with the $[IrCl_6]^{2-}$ reactant. With reactions selective for the tris-pyalk species, yields of mono- and bis-chelate species were low to trace. Complex **8** was prepared in this manner, as reported previously,[27] in poor yield (8%, Scheme 3). The same reported reaction also produced very small amounts of **3–7** (below 1% for most), which was unfeasible for bulk preparation.

Inspired by an unrelated organic synthesis protocol in which partially substituted species were best accessed *via* excision from a fully substituted compound,[28] we treated an unseparated mixture of the tris-pyalk isomers **1** and **2** with 1 M HCl in acetone under microwave heating in a pressure vessel, followed by the same oxidation and extraction procedure as before; the initial product mixture is always in the Ir(III) state, presumably due to the acidic conditions. With appropriate timing – at least 20 minutes at 120 °C – the product mixture yielded good conversion to all five bis-pyalk isomers (**3–7**), but no detectable traces of **8** even at longer times. Selection of temperature and heating time was important for optimizing the reaction; shorter runs or cooler temperature resulted in incomplete ligand excision, while longer runs altered the composition of products, notably with the depletion of **7**. Under our preferred reaction conditions, complex **6** was nearly an order of magnitude more abundant than the other isomers, which were of comparable abundance (Scheme 3). Additionally, we find that higher concentrations of starting material (and HCl, proportionally) over our preferred conditions (50 mM) result in drastically lower conversion, with much of the starting material left unreacted.

Isolation of the mixed compounds $\mathbf{3^{IV}}$–$\mathbf{7^{IV}}$ can easily be accomplished by silica gel chromatography, using various mixtures of hexane, dichloromethane, ethyl acetate, and acetone. The elution order of the products varies considerably depending on the eluent, but in all cases **3** elutes first and **6** last. Specific eluent composition is, therefore, important, as some blends result in overlapping products. We saw good results with 25% ethyl acetate in dichloromethane, the latter being vital for avoiding solubility problems; this resulted in the elution sequence **3-5-7-4-6**. Overlap of the trailing end of the **4** band with **6** was a common problem, although the latter could be purified by repeatedly dissolving in dichloromethane and precipitating with hexane, as the former remains soluble in less

Table 1 Qualitative descriptions of complexes **1–8** in the Ir(IV) state

Compound	Geometry (point group)	Appearance (1 mM)	Solvent range	Redox behavior[a]
1 (PF_6^-/Cl^-)	Meridional (C_1)	Orange	Any non-hydrocarbons	Spontaneous oxidation (minutes-hours)
2 (PF_6^-/Cl^-)	Facial (C_3)	Scarlet	Any non-hydrocarbons	Spontaneous reduction (hours)
3	*trans*-Cl *trans*-O *trans*-N (C_{2h})	Magenta	Dichloromethane (~1 mM max), dichloroethane, acetone (poorly)	Spontaneous oxidation (minutes)
4	*cis*-Cl *cis*-O *trans*-N (C_2)	Emerald green	Non-hydrocarbon organics, sparingly in water	Near-bistable, gradual oxidation (hours-days)
5	*cis*-Cl *trans*-O *cis*-N (C_2)	Orange-yellow	Non-hydrocarbon organics, sparingly in water	Stable Ir(IV), unstable Ir(III) (difficult to form, degrades)
6	*cis*-Cl *cis*-O *cis*-N (C_1)	Red	Non-hydrocarbon organics, sparingly in water	Converge to mixed Ir(III/IV)
7	*trans*-Cl *cis*-O *cis*-N (C_{2v})	Maroon	Dichloromethane, acetone	Near-bistable, gradual reduction (hours-days)
8 (Na^+ salt)	Single isomer (C_s)	Dull green	Water, polar organics (ethyl acetate, acetone, *etc.*)	Bistable Ir(III/IV)

[a] The final column describes spontaneous Ir(III/IV) redox behavior when compounds are handled under ambient atmosphere and temperature, using standard research-grade commercial solvents. Oxidation refers to initially reduced [Ir(III)] samples.

polar solvent mixtures. Chromatography of these species is greatly aided by their intense and characteristic colors, resulting in visually obvious elution bands of even tiny (<1 mg) amounts (Fig. S1†).

Table 1 lists qualitative descriptions of complex-specific properties of **1–8**: isomer geometry, molecular symmetry, appearance, solubility, and redox behavior. In addition to these, complexes **3–8** share some common properties. Like **1** and **2**, the new compounds are readily oxidized to the Ir(IV) state by sodium periodate, showing no signs of degradation. These oxidized species are long-lived in the solid state, as well as in organic solvents not prone to oxidation: dichloromethane, acetone, ethyl acetate, and pure alkanes gave good lifetimes (>1 day at room temperature), whereas oxidizable solvents like non-tertiary alcohols slowly reduced most of the compounds.

Despite the fact that **3–8** are initially formed as Ir(III) species prior to oxidative workup, deliberate reduction of the isolated Ir(IV) complexes proved troublesome. We found that oxidizable primary and secondary alcohols, particularly refluxing isopropanol, successfully reduced our complexes to the Ir(III) state. NMR spectroscopy of the resulting products (ESI Section III†) indicated mixed results: $\mathbf{4}^{\mathbf{III}}$, $\mathbf{7}^{\mathbf{III}}$ and $\mathbf{8}^{\mathbf{III}}$ each show a single pure diamagnetic product with the expected number of ligand peaks for each geometry. Reduction of **6** results in a mostly diamagnetic, air-sensitive species with slightly broadened NMR peaks (Fig. S4†), presumably due to incomplete reduction despite handling in inert atmosphere, while **3** and **5** produced air-sensitive mixtures of multiple species. Only two reduced species, $\mathbf{4}^{\mathbf{III}}$ and $\mathbf{6}^{\mathbf{III}}$, were successfully crystallized. Use of more conventional reductants, like ascorbate or zinc powder, generally yielded worse results. We suspect that the difficulties in obtaining pure Ir(III) species lie in the combined presence of alkoxo and chloro ligands, as the former is basic on Ir(III) and the latter is susceptible to basic hydrolysis. However, we can still regenerate the starting Ir(IV) species by treatment with HCl followed by oxidation. Because of these problems with the Ir(III) state, we emphasize the better-behaved Ir(IV) species here.

Structural characterization

All of the complexes in the Ir(IV) state, as well as **4** and **6** in the Ir(III) state, were successfully crystallized and structurally characterized by X-ray crystallography (Fig. 2). M–L bond lengths (ESI Section IV†) are similar to those in $\mathbf{1\text{-}2}^{\mathbf{IV}}$. Ir–O bond lengths of $\mathbf{3\text{–}8}^{\mathbf{IV}}$, known to vary with oxidation state,[22] were all around 1.95 ± 0.02 Å, corresponding to Ir(IV). Trans effects are difficult to ascertain, as the overall M–L bond length variation across all complexes (up to 0.05 Å) is comparable to variations among molecularly (but not crystallographically) symmetric bonds (up to 0.02 Å), as well as same *trans*-ligand arrangements across different isomers (0.03 Å), indicating that crystal packing effects and/or structure solution uncertainty are within the same range. In the two Ir(III) structures we obtained, $[\mathbf{4}^{\mathbf{III}}]$H and $[\mathbf{6}^{\mathbf{III}}]$H, we modeled the complexes as neutral species protonated at one of the alkoxo groups (disordered over each one), since in both cases there was no cation in the structure. One water molecule hydrogen bonds strongly to the protonated and deprotonated alkoxo groups of adjacent complexes, as evidenced by the approximately 2.6 Å O–O distance to each ligand atom in both structures. The Ir–O bond lengths were similar (2.01–2.08 Å), which we attribute to the disordered protonation of both Ir–O motifs in the solid state that were accordingly modeled (*ca.* 60 : 40) leading to two related H-bonding patterns for each

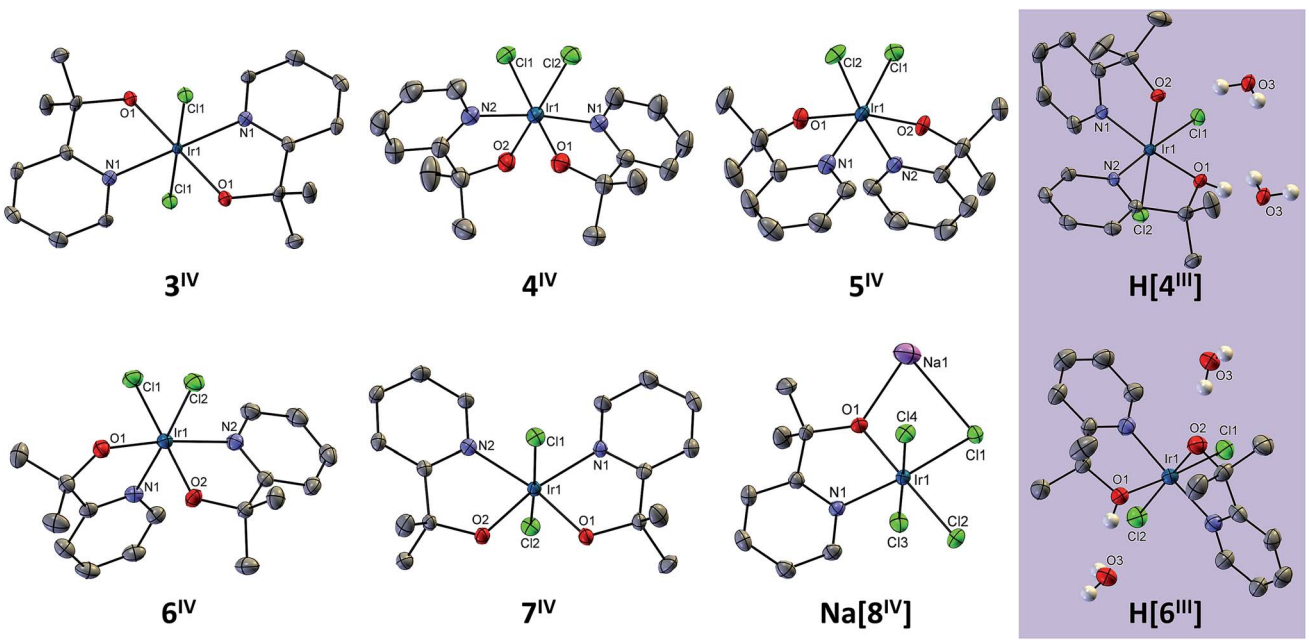

Fig. 2 ORTEP crystal structures of $\mathbf{3\text{–}8}^{\mathbf{IV}}$ and $\mathbf{4}^{\mathbf{III}}$ and $\mathbf{6}^{\mathbf{III}}$ drawn at the 50% probability level. Solvent molecules are omitted for clarity, except for the water molecules in the Ir(III) structures. Hydrogen atoms are similarly omitted, except at alkoxo positions (all alkoxos are deprotonated unless explicitly drawn). Drawings of $\mathbf{4}^{\mathbf{III}}$ and $\mathbf{6}^{\mathbf{III}}$ both show one of two disordered states, the other having a proton at O2 instead of O1.

monoprotonated Ir(III) structure. In comparison with the Ir(IV) structures, we observe that the Ir–O bonds are over 2 Å: 2.02 and 2.08 Å for $\mathbf{4}^{\mathbf{III}}$ as compared to 1.95 and 1.94 Å for $\mathbf{4}^{\mathbf{IV}}$, and 2.01 and 2.07 Å for $\mathbf{6}^{\mathbf{III}}$ as compared to 1.96 and 1.95 Å for $\mathbf{6}^{\mathbf{IV}}$. The Ir–N bonds are only slightly shortened, by about 0.03 Å, and there is no clear trend with the Ir–Cl bonds.

All complexes have an octahedral geometry, but distorted due to the 80–82° bite angle of pyalk. In **7**, there is a very clear interligand steric clash: the *cis*-pyridine ligands are coplanar, forcing their 6-H atoms close together. This is evident from the sub-van-der-Waals H–H contact of ~2.0 Å, as well as the distended 111° N–Ir–N bond angle. With four sterically unproblematic alternative structures available, it is surprising that this isomer forms, survives the high (120–130 °C) temperatures, and is present in similar yields to three of the other isomers. In fact, under slightly modified conditions (20 min at 120 °C), complex **7** was the second most abundant isomer, with a 13% isolated yield.

Spectroscopy

All of $\mathbf{3}$–$\mathbf{8}^{\mathbf{IV}}$ have intense (2000–4000 M^{-1} cm^{-1}) visible absorption bands (Fig. 3) typical for LMCT in Ir(IV); complexes $\mathbf{3}$–$\mathbf{5}^{\mathbf{IV}}$ also show a much weaker near-IR feature. The spectra differ strongly, indicating that the frontier electronic levels are highly affected by ligand orientation. TD-DFT calculations (see below) modeled the absorption features fairly well, though with an overall red-shift of 50–100 nm, which is expected due to the definiteness of the approach.[29] Natural transition orbital analysis (ESI Section VII†) suggests that the dominant visible LMCT excitations come primarily from delocalized ligand MO's (mainly Cl and O p orbitals) exciting into the half-filled Ir-centered d_π valence orbital.

Electrochemistry

Cyclic voltammetry (CV) was performed on compounds **3**–**8** in dichloromethane, as it is one of the few solvents to properly dissolve all of them, as shown in Table 1 (although the sodium salt of **8** does not dissolve well in the pure solvent, ion exchange with the electrolyte solubilizes it). Complexes **4** and **8** were also measured in water due to their solubility; because we suspect that avoiding pyalk protonation requires basic conditions as for **1** and **2**,[22] the solution was kept neutral to prevent chloride hydrolysis.

All of the complexes display a single reversible or quasi-reversible feature (Table 2). We assign this to the 'pure' $Ir^{IV/III}$ couple for a number of reasons. One, the aprotic solvent should prevent the alkoxide groups from protonating upon reduction. Similarly, the noncoordinating solvent and electrolyte are unlikely to displace the chloro ligands. Finally, cyclic voltammetry occurs on the order of seconds at room temperature, whereas our bulk reduction attempts involved elevated temperatures for at least 5–10 min. As for the two aqueous measurements, protonation is a likely factor, as it was for **1** and **2**, but aside from that, **4** and **8** showed stable reduction behavior; nonetheless, their potentials are only given as rough indications for the aqueous-phase redox trend in reducing the number of pyalk substituents.

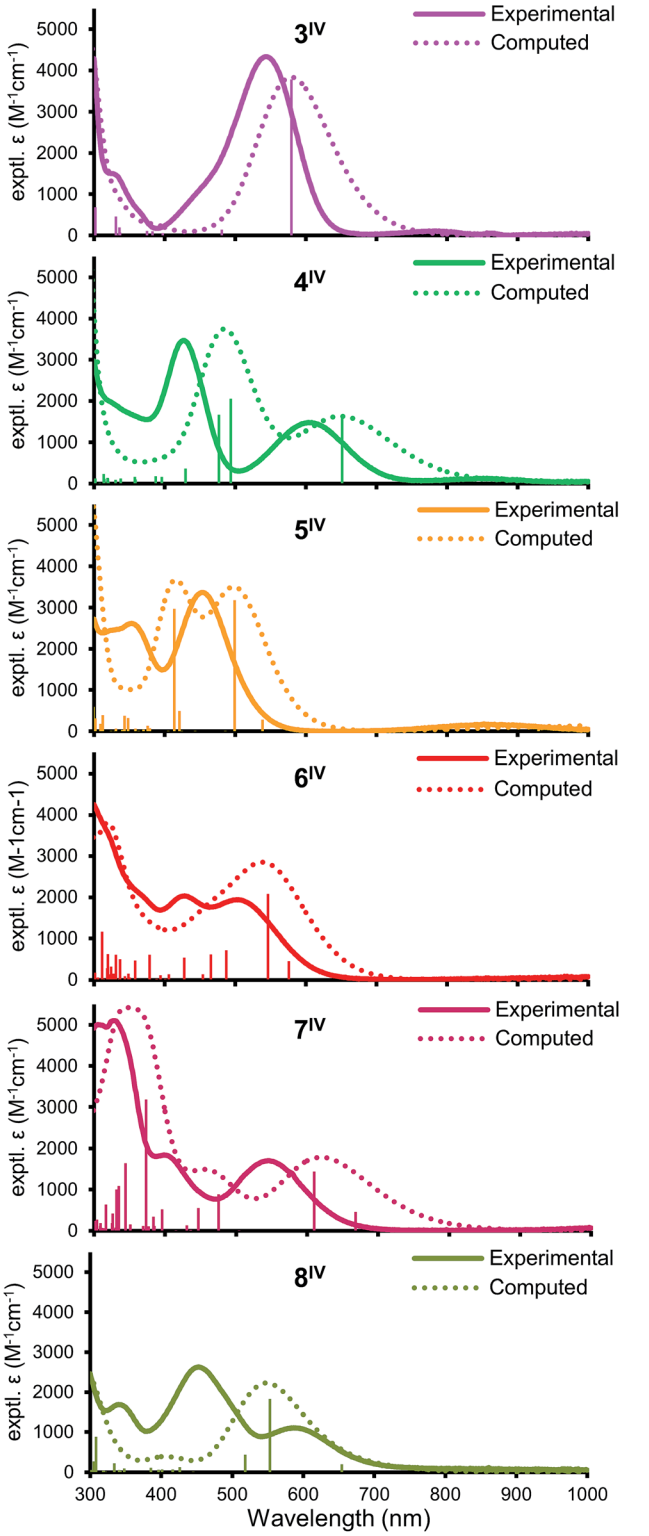

Fig. 3 Experimental UV-visible spectra (solid), along with DFT-computed spectra (dotted) and corresponding excitations (vertical lines) for $\mathbf{3}^{\mathbf{IV}}$–$\mathbf{8}^{\mathbf{IV}}$ in dichloromethane (1 : 1 ethyl acetate/dichloromethane for $\mathbf{8}^{\mathbf{IV}}$). Absolute DFT intensities are arbitrarily scaled.

The data clearly demonstrate the comparatively high stability of the Ir(IV) state both in organic and aqueous environments. The extreme case is complex **3**, with an $Ir^{IV/III}$

Table 2 Electrochemical data for the studied complexes in aqueous and dichloromethane solutions

Complex	$Ir^{IV/III}$ $E_{1/2}$ aq.[a] (mV *vs.* NHE)	$Ir^{IV/III}$ $E_{1/2}$ DCM[b] (mV *vs.* NHE)	Theor. HOMO plane
1	426[c]	194[c]	NOOO
2	799[c]	528[c]	NNOO
3		15	ClClOO
4	483	95	ClClOO
5		183	NClOO
6		304	NClOO
7		317	NClClO
8	765	212	ClClClO
$[IrCl_6]^{2-}$	910[d]		ClClClCl

[a] Potentials for 0.1 M aqueous KNO_3 solution (pH 7); converted from Ag/AgCl reference by 197 mV offset. [b] Potentials for 0.1 M NBu_4PF_6 dichloromethane solution; converted from Fc^+/Fc reference by 704 mV offset.[30] [c] Ref. 22. [d] Ref. 7.

potential of only 15 mV *versus* NHE. Another notable trend, the considerable shift in potentials between aqueous and organic solutions, may result from alkoxide-water hydrogen bonding and net charge change. Although **3–8** have fewer pyalk ligands than **1-2**, this does not on average increase the $Ir^{IV/III}$ potential in dichloromethane, despite pyalk being a stronger donor than chloride. Since species with lower net charge are preferred in nonpolar solutions, the solvent environment hinders oxidation of **1** and **2** while promoting oxidation of **3–8**. As a result, we avoid direct comparisons between isomer sets.

In agreement with qualitative observations and following the trend of **1** and **2**, isomers **3–7** span a range of just over 300 mV in $Ir^{IV/III}$ potentials. Although we now have a more complicated ligand sphere, the ligand-field model still correctly predicts the overall trend. First, the ligand donor strengths are ordered N < Cl < O, based on our data as well as ligand parameters.[19,20,24,25] The d orbital that experiences the greatest net ligand donation becomes the HOMO that gives the oxidation enhancement effect; Table 2 shows the resulting pattern.

There is one point of ambiguity in ranking these planes: the relative donor strength of 2 × Cl *versus* N + O. The observation that pyalk overall is a stronger donor indicates that donation should follow Cl + Cl < N + O. This relation is only relevant in the case of **7**, which is nearly isotropic, having one plane containing ligands NNOO and two planes with NClClO. We would expect the former to correspond to the highest d orbital, but our DFT calculations indicate the opposite ordering, as discussed below. Regardless, the ordering predictions are the same: **3** and **4** are the most easily oxidized, followed by **5** and **6**, while **7** is the most difficult. Within each group, however, there are notable deviations: the potentials for **5** and **6** differ by 121 mV, while **3** and **4** differ by 80 mV. For the former pair, our DFT electronic structure calculations (see below) suggest a reason: **5** possesses a degenerate pair of high-energy planes (NClOO). However, the two corresponding molecular orbitals are non-degenerate hybrids oriented along the (non-degenerate) diagonals between those two planes; this degeneracy break elevates one of the orbitals, thus lowering the $Ir^{IV/III}$ potential. As for **3** and **4**, we are uncertain as to the exact origin of the difference, but we note that **3** is the most anisotropic complex, having maximally differentiated orbital planes (ClClOO, NNOO, NNClCl), whereas **4** has two degenerate lower levels (NNClO).

In order to further ascertain the validity of the ligand-field treatment approach, we investigated the redox properties of **3–7** with DFT calculations (B3LYP/def2TZV, 6-311+G(d, p)//B3LYP/def2SVP, 6-31+G(d, p)). Table 3 presents the computed relative potentials derived from the two approaches discussed above: the difference of relative free energies of the Ir(III) and Ir(IV) states, as well as the relative ionization energy of the Ir(III) HOMO. It is evident that the full thermodynamic treatment gives much better experimental agreement: with an average deviation of 34 mV, the measured isomer dependence pattern is captured very well. The reduced-state HOMO method is noticeably cruder, giving larger deviations and swapping the order of the closely spaced **6** and **7**. Nonetheless, it also captures the general redox trend, demonstrating that relative redox properties can be estimated from the frontier electronic level, at least in this case.

Thermodynamic properties

The relative thermodynamic stability of the isomer series is relevant to understanding the inertness of Ir(IV). As noted above, the comparable abundances of all isomers in the reaction products could either mean that the product distribution is kinetically controlled with very slow exchange kinetics or that the complexes reach equilibrium and have nearly equal energy. The calculations mentioned above are useful here: Table 4 shows the relative ordering of **3–7** in the Ir(III) and Ir(IV) states. For Ir(IV), the order of thermodynamic stability parallels that of the $Ir^{IV/III}$ potentials, with **3** being the lowest and **7** the highest in energy. Compared with the Boltzmann population rates of 1.36 and 1.80 kcal mol^{-1} per concentration decade at 25 °C and

Table 3 DFT potentials relative to **3**, computed from free energies (middle) and reduced state HOMO energy (right), compared with experimentally measured values (left)

Complex	Expt. $Ir^{IV/III}$ $E_{1/2}$ in DCM relative to **3** (mV)	Theor. $Ir^{IV/III}$ E_{red} in DCM relative to **3** (mV)	Ir^{III} HOMO energy relative to **3** (meV)
3	0	0	0
4	80	119	135
5	168	143	267
6	289	317	448
7	302	378	422

Table 4 Free energies in kcal mol^{-1} for **3–7** in each oxidation state relative to compound **3**

Complex	Relative energy for Ir^{III} (kcal mol^{-1})	Relative energy for Ir^{IV} (kcal mol^{-1})
3	0	0
4	−1.19	1.55
5	3.23	6.53
6	1.47	8.80
7	5.79	14.52

120 °C, respectively, we see that the spread of computed energies is several times greater. This spread is smaller for Ir(III) (the state in which these products are formed in the reaction), in line with the similar ordering of redox potentials, but would nonetheless be sufficient to effectively eliminate many of the species if formation was under thermodynamic control. The inertness of Ir(III) is well known, however, so we turn to the Ir(IV) case. The energies predict that an equilibrium distribution would consist mostly of **3**, with **4** being an order of magnitude less abundant, and the other compounds occurring in negligible amounts. Instead, we see inert behavior, as pure samples of each isomer have not shown interconversion on storage over weeks at room temperature or a year at −20 °C. In fact, isomerization only becomes detectable at temperatures approaching 100 °C and reaction times of minutes to hours.

Electronic structure and EPR

Since Ir(IV) is an odd-electron low spin d^5 state with $S = 1/2$, we attempted to obtain frozen solution EPR spectra for **1–8**. While we were able to obtain spectra for **1**, **3**, **4**, **5**, and **8** (Fig. 4), compounds **2**, **6**, and **7** gave no discernible signal despite multiple attempts using various solvent conditions, temperatures and microwave powers. Each observed spectrum was successfully simulated (Fig. 4) as an $S = 1/2$ system with significant g anisotropy (Table 5). All spectra are very anisotropic, to the point that some features were difficult to assign without the help of these empirical simulations. This anisotropy is consistent with Ir(IV) as opposed to ligand-centered radicals.

The spectra of **1** and **3** show rhombic EPR signals, as expected from their geometries. Although both exhibit minor structure in the g_z peak, it could not be simulated satisfactorily as hyperfine coupling to any of the available nuclei. Instead, we simulated all of the spectra with unresolved hyperfine coupling. Complex **4** gives an axial spectrum, although the g_z turning point has very low amplitude; assignment was made possible by optimizing the lineshape of the main absorption; doing so gave a simulated g_z peak whose intensity agrees well with the observed feature. The axial symmetry is expected based on the geometry, as the two filled d_π levels are in a degenerate ligand environment. Complexes **5** and **8** give rhombic spectra with very low g_z values; the g_z turning points were undetectable and estimated from the simulations to be <1.2. These parameters indicate three distinct d_π levels, but with less separation than in the first three cases. As for the remaining species, there are

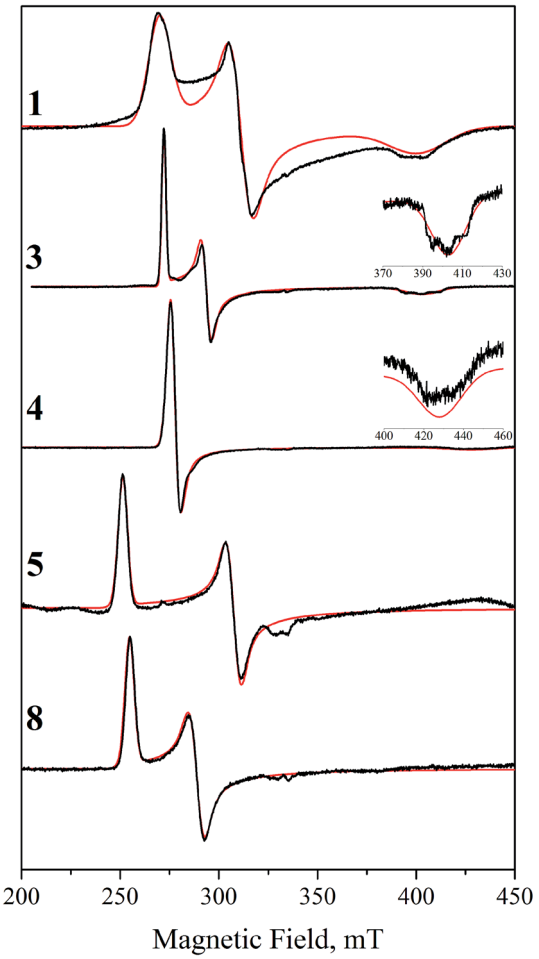

Fig. 4 X-band EPR spectra for Ir(IV) species in glassed frozen solutions (black) and corresponding simulated spectra (red). Inserts are provided for the high-field peaks of **3** and **4**. Note that features near 330 mT are due to trace Cu(II) contamination.

a number of reasons why they may not show an EPR signal, such as aggregation. The most likely one, however, as discussed below, is that the spin–orbit coupling is too great and broadens the signals beyond detection, since DFT calculations show that the lower d_π states lie closer in energy to the valence level in these complexes than in the others. Despite the lack of EPR signals, NMR spectroscopy clearly indicates paramagnetism, as spectra of $[\mathbf{2}^{\mathbf{IV}}]^+$ and $\mathbf{6}^{\mathbf{IV}}$ show broad paramagnetic peaks very similar to those of $[\mathbf{1}^{\mathbf{IV}}]^+$ (Fig. S7–S9†).

Our DFT data help us explain the implications of these results by analyzing the computed electronic structures. Fig. 5

Table 5 Simulated EPR parameters

	g_x	g_y	g_z	g_{iso}	H_x, MHz	H_y, MHz	H_z, MHz
1	2.484	2.153	1.668	2.102	454	345	781
3	2.464	2.283	1.662	2.136	71.4	155	473
4	2.423	2.422	1.564	2.136	140	227	551
5	2.658	2.172	<1.2		185	201	>1000
8	2.627	2.317	<1.2		180	230	>1000

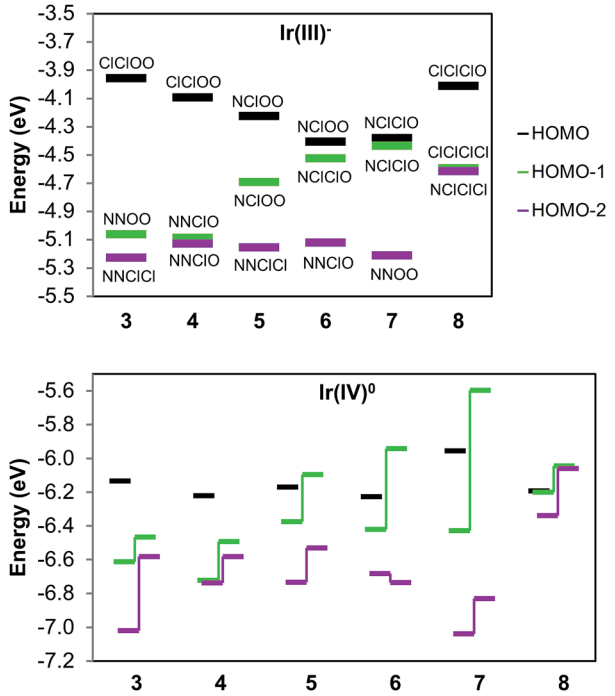

Fig. 5 Computed energies for the three frontier occupied electronic levels (Ir-centered t_{2g} orbitals) of **3–8** in each oxidation state, labeled with their corresponding coplanar ligands (same legend and labeling applies to both graphs). Bottom: alpha and beta spin levels correspond to leftward and rightward bars, respectively; paired levels are connected by vertical lines and color (the virtual beta SOMO is not shown).

presents the Ir d frontier energy levels for each complex in the anionic Ir(III) and neutral Ir(IV) oxidation states. The three highest-occupied molecular orbitals (ESI Sections V and VI†) are primarily delocalized antibonding combinations of Ir d_π orbitals with Cl and O p orbitals, with a dominant contribution from the metal. Similarly to what we previously calculated for **1** and **2**, the Ir(IV) spin density ranges within 0.52–0.57 for each isomer, indicating high covalency and delocalization in the coordination bonds. We also observe that the three frontier levels are ordered as predicted by ligand-field theory, with a few small caveats. For one, the energy ordering is more difficult to interpret in the Ir(IV) state than in the Ir(III) state as the alpha and beta spin levels are highly split by spin polarization effects. Therefore, the closed-shell calculations are helpful in clearly illustrating the ligand environment's effects, despite involving a different oxidation state than our isolated products. Complexes **3**, **4**, **6**, and **8** show expected patterns, with the ligand-field predicted orbital ordering. It can be deduced that the O and Cl ligands have a more similar impact to each other than N does, since MO's that are differentiated by O–Cl changes are closer in energy than ones differentiated by N–Cl changes (**3**, **6**, and **8** display this clearly). This is reasonable, given that both chloro and alkoxo are anionic ligands, whereas pyridine is neutral.

As mentioned previously, the MO levels for **5** and **7** are less straightforward to interpret. In **7**, the plane ordering is swapped from the initial guess that Cl + Cl < N + O. It appears from what we noted above (that Cl is closer to O than N) that in terms of electronic perturbation this inequality is reversed, despite the fact that the N, O pair of ligands promotes high oxidation states more than two Cl ligands do. Another possible explanation is that the alkoxides' atomic p orbitals are perpendicular to the NNOO plane, rendering them unable to mix with that d orbital, thus decreasing the antibonding interaction. Given this, both complexes also have a degenerate pair of frontier planes, NClOO for **5** and NClClO for **7**. In both cases, the resulting MO's are combinations of the degenerate d orbitals and occupy the diagonal positions. Interestingly, this has drastically different impacts on each isomer. In **7**, these "hybrid" MO's remain very similar in energy, while in **5** they diverge considerably. Although both diagonal planes have the same on-plane and off-plane ligands, the different orientations affect the allowed ligand–metal π^* delocalization for each orbital.

This electronic structure rationalizes the EPR results by analogy with low-spin octahedral Fe(III). Thus, the *g*-value anisotropy is attributed to spin–orbit coupling, from mixing of the SOMO with other MOs close in energy to create states with nonzero orbital angular momentum. This relies on the typical assumption that, due to energetic proximity, only the other two d_π orbitals contribute significantly. Since the effect is inversely proportional to the energy gap, the overall *g*-anisotropy is expected to be inversely related to the ligand-field anisotropy of the compound. The least anisotropic spectra we obtained were those of **1**, **3**, and **4**, since all *g*-value peaks are well-resolved. As discussed here and in our previous work, these complexes have the most anisotropic arrangements possible for their respective ligand sets. Despite the high ligand-field anisotropy that splits the d_π orbitals, the observed spectra are nonetheless still very anisotropic, underscoring the high spin–orbit coupling that Ir(IV) displays.

As the MO separation decreases further for the remaining species, the EPR spectra broaden past the point of detection. Complexes **5** and **8** model as rhombic signals, but with g_z too low to detect. And finally, the three cases that showed no detectable signal, **2**, **6**, and **7**, can be potentially explained. These are the complexes with the least anisotropic valence shell; more specifically, each has a filled orbital very close in energy to the HOMO. Therefore, the lack of apparent signal is likely due to broadening from excessive spin–orbit coupling.

In summary, we find that our Ir(IV) EPR spectra correlate well with computed electronic structures. As a specific example, the observation that **5** gives a rhombic signal was helpful since it validates the calculated electronic structure, showing that electronic arrangement is not easily predicted from ligand geometry when the structure has degenerate *d* planes. We also observe that Ir(IV) has a very high spin–orbit coupling constant: Ir(IV) spectra are dramatically broader than the spectra of the closely related Rh(IV) complexes'. For example, our Rh analogue of **1** gave a spectrum spanning 35 mT, roughly five times less than that of **1**.[23] This anisotropy can impact the observation of a signal when the t_{2g} orbitals are close in energy; therefore, lack of EPR activity should not be considered conclusive evidence for the absence of a mononuclear Ir(IV) species.

Conclusions

We have prepared, isolated, and studied a rare complete set of five isomers of $Ir(pyalk)_2Cl_2$, found to be stable Ir(IV) compounds. These complexes exhibit remarkable kinetic stability, allowing for facile handling of pure species. Like our previously reported $Ir(pyalk)_3$ isomers, they exhibit dramatic electronic disparities, with $Ir^{IV/III}$ potentials spanning over 300 mV. We were able to qualitatively explain the isomer dependence in terms of ligand-field theory and investigated relevant electronic structures quantitatively with DFT calculations. In addition, we measured EPR spectra in order to further explore the electronic structure as well as to expand upon the scarce Ir(IV) EPR literature.

This report has a number of significant implications. First, the exceptional substitutional inertness that is observed in our Ir(IV) species supports the hypothesis that our WOCs can be composed of many, non-interconverting species regardless of predicted thermodynamic energy differences.[10] Furthermore, we observe that this isomerism has implications beyond simply complicating characterization – the highly anisotropic nature of the pyalk ligand can be expected to affect the redox properties of each WOC isomer to a substantial degree, much as we see with **1–8**. For a complex oxidative process such as water oxidation, the catalyst's redox transitions are of critical importance; we would, therefore, expect that isomerism could play a significant role in the catalytic activities of individual species, which would thus be expected to differ considerably in redox and catalytic properties.

Although our results are not directly related to any proposed Ir WOC species, we aim to synthesize more catalytically relevant oxo-bridged dinuclear analogues. With the new series of Ir-pyalk monomers now separately available, the synthesis of single isomers of the dinuclear species is made possible. Further work will focus on formation of bridging oxo groups in order to make such dimer analogues from monomeric bis-pyalk Ir complexes. By having an additional pyalk ligand on each Ir atom, and being able to start with pure isomers, the separation and isolation problems encountered with the activated Cp*Ir WOC mixture (excessive isomers, binding to solids, *etc.*) may be circumvented.

Acknowledgements

This work was supported as part of the Argonne-Northwestern Solar Energy Research (ANSER) Center, an Energy Frontier Research Center funded by the U.S. Department of Energy, Office of Science, Office of Basic Energy Sciences, under Award Number DE-SC0001059. V. S. B. acknowledges supercomputing time from the High Performance Computing facilities at Yale University and at NERSC. B. R. acknowledges support from the National Science Foundation Graduate Research Fellowship under Grant No. DGE-1122492. The authors would like to thank Drs Svante Hedström and Ke R. Yang for helpful advice.

Notes and references

1 S. R. Klei, T. D. Tilley and R. G. Bergman, *J. Am. Chem. Soc.*, 2000, **122**, 1816.
2 K. Kawamura and J. F. Hartwig, *J. Am. Chem. Soc.*, 2001, **123**, 8422.
3 K. J. H. Young, O. A. Mironov and R. A. Periana, *Organometallics*, 2007, **26**, 2137.
4 K. C. Fortner, D. S. Laitar, J. Muldoon, L. Pu, S. B. Braun-Sand, O. Wiest and S. N. Brown, *J. Am. Chem. Soc.*, 2007, **129**, 588.
5 K. R. Yang, A. J. Matula, G. Kwon, J. Hong, S. W. Sheehan, J. M. Thomsen, G. W. Brudvig, R. H. Crabtree, D. M. Tiede, L. X. Chen and V. S. Batista, *J. Am. Chem. Soc.*, 2016, **138**, 5511.
6 A. B. Tamayo, B. D. Alleyne, P. I. Djurovich, S. Lamansky, I. Tsyba, N. N. Ho, R. Bau and M. E. Thompson, *J. Am. Chem. Soc.*, 2003, **125**, 7377.
7 S. Petrovic, *Chem. Educ.*, 2000, **5**, 231.
8 N. D. Schley, J. D. Blakemore, N. K. Subbaiyan, C. D. Incarvito, F. D'Souza, R. H. Crabtree and G. W. Brudvig, *J. Am. Chem. Soc.*, 2011, **133**, 10473.
9 U. Hintermair, S. M. Hashmi, M. Elimelech and R. H. Crabtree, *J. Am. Chem. Soc.*, 2012, **134**, 9785.
10 U. Hintermair, S. W. Sheehan, A. R. Parent, D. H. Ess, D. T. Richens, P. H. Vaccaro, G. W. Brudvig and R. H. Crabtree, *J. Am. Chem. Soc.*, 2013, **135**, 10837.
11 S. W. Sheehan, J. M. Thomsen, U. Hintermair, R. H. Crabtree, G. W. Brudvig and C. A. Schmuttenmaer, *Nat. Commun.*, 2015, **6**, 6469.
12 J. M. Thomsen, S. W. Sheehan, S. M. Hashmi, J. Campos, U. Hintermair, R. H. Crabtree and G. W. Brudvig, *J. Am. Chem. Soc.*, 2014, **136**, 13826.
13 D. L. Huang, R. Beltrán-Suito, J. M. Thomsen, S. M. Hashmi, K. L. Materna, S. W. Sheehan, B. Q. Mercado, G. W. Brudvig and R. H. Crabtree, *Inorg. Chem.*, 2016, **55**, 2427.
14 A. Savini, P. Belanzoni, G. Bellachioma, C. Zuccaccia, D. Zuccaccia and A. Macchioni, *Green Chem.*, 2011, **13**, 3360.
15 C. Zuccaccia, G. Bellachioma, S. Bolano, L. Rocchigiani and A. Savini, *Eur. J. Inorg. Chem.*, 2012, 1462.
16 C. Zuccaccia, G. Bellachioma, O. Bortolini, A. Bucci, A. Savini and A. Macchioni, *Chem.–Eur. J.*, 2014, **20**, 3446.
17 S. E. Castillo-Blum and A. G. Sykes, *Polyhedron*, 1987, **6**, 101.
18 A. Cusanelli, U. Frey, D. T. Richens and A. E. Merbach, *J. Am. Chem. Soc.*, 1996, **118**, 5265.
19 S. A. DiFranco, N. A. Maciulis, R. J. Staples, R. J. Batrice and A. L. Odom, *Inorg. Chem.*, 2012, **51**, 1187.
20 R. D. Bemowski, A. K. Singh, B. J. Bajorek, Y. DePorre and A. L. Odom, *Dalton Trans.*, 2014, **43**, 12299.
21 M. E. Jung and G. Piitzi, *Chem. Rev.*, 2005, **105**, 1735.
22 D. Y. Shopov, B. Rudshteyn, J. Campos, V. S. Batista, R. H. Crabtree and G. W. Brudvig, *J. Am. Chem. Soc.*, 2015, **137**, 7243.
23 S. B. Sinha, D. Y. Shopov, L. S. Sharninghausen, D. J. Vinyard, G. W. Brudvig and R. H. Crabtree, *J. Am. Chem. Soc.*, 2015, **137**, 15692.
24 A. B. P. Lever, *Inorg. Chem.*, 1990, **29**, 1271.
25 L. Perrin, E. Clot, O. Eisenstein, J. Loch and R. H. Crabtree, *Inorg. Chem.*, 2001, **40**, 5806.
26 H. Masui and A. B. P. Lever, *Inorg. Chem.*, 1993, **32**, 2199.

27 K. Materna, B. Rudshteyn, B. J. Brennan, M. H. Kane, A. Bloomfield, D. Huang, D. Y. Shopov, V. S. Batista, R. H. Crabtree and G. W. Brudvig, *ACS Catal.*, 2016, **6**, 5371.
28 P. P. Castro, G. Zhao, G. A. Masangkay, C. Hernandez and L. M. Gutierrez-Tunstead, *Org. Lett.*, 2004, **6**, 333.
29 A. Jesser, M. Rohrmuller, W. G. Schmidt and S. Herres-Pawlis, *J. Comput. Chem.*, 2014, **35**, 1–17.
30 N. G. Connelly and W. E. Geiger, *Chem. Rev.*, 1996, **96**(2), 877.